# Pore Structure and Liquid Behavior of Nonwovens Composed of Nanosized Fibers by Conjugate Spinning

**Yue Li, Chang Whan Joo**

*Department of Organic Materials and Textile System Engineering, Chungnam National University, Daejeon 305-764, Korea*

Received 16 August 2011; accepted 5 December 2011
DOI 10.1002/app.36627
Published online in Wiley Online Library (wileyonlinelibrary.com).

**ABSTRACT:** Nonwovens composed of nanofibers are of interest for use in high-function textile materials, such as filtration, insulation, and absorption media. The pore structure of nonwovens has a dominant influence on the performance characteristics of the final products, particularly in controlling the transport properties. The transport properties include the filtration of gas and liquid, sound absorption, and heat transfer. In this study, we focused on the pore structure and liquid behavior of needle-punched nonwovens composed of nanofibers produced by conjugate spinning. Nanofiber nonwovens were prepared with poly(ethylene terephthalate)/co-(polyethylene terephthalate) sea-island bicomponent fibers by an alkali treatment. The pore diameter distributions were experimentally obtained with a capillary flow porosimeter; this indicated that the nonwovens composed of nanofibers had a compact and uniform textile structure. Moreover, a comparison of the pore diameters, water absorption, and wicking behaviors of the nonwovens before and after the alkali treatment was made. The nonwovens composed of nanofibers possessed excellent water absorption capacities and fast wicking behaviors. Thus, they have promising potential applications as absorption media. In addition, a theoretical model of air volume and channel radius for liquid behavior was established and compared with the experimental results. © 2012 Wiley Periodicals, Inc. J Appl Polym Sci 000: 000–000, 2012

**Key words:** fibers; polyesters; structure–property relations; voids

## INTRODUCTION

The needle-punching technique is a mechanical bonding method for producing nonwovens. Fibers are mechanically entangled to produce a fabric with reciprocating barbed needles through a moving web in a needle loom. In this method, the characteristics of nonwovens can be altered under various processing conditions; these characteristics include the stroke number, penetration depth, production velocity, and needle design.[1] The applications of needle-punched nonwovens are wide ranging and extend into many niche product areas. However, nonwovens composed of nanofibers are major media with limited applications, such as filtration, insulation, and absorption media.

The pore geometry in nonwovens can be represented as a three-dimensional structure of pores connected by fibers. The pores inside the nonwovens are highly complex in terms of size, shape, and capillary geometry.[2–4] The pore diameter and its distribution in nonwovens affect the transport behaviors, including air permeability, liquid absorption, wicking behavior, and filtration efficiency.

Nonwovens consisting of sea-island or split bicomponent fibers are used, in particular, to prepare ultrafine fibers or nanofibers by alkali treatment or hydroentanglement, respectively.[5–9] Recently, nonwovens composed of nanofibers have been paid more attention in numerous fields because they offer unique advantages, including a softer hand, high absorbency, and high filtration efficiency, because of their high specific surface area and small pore size.

To determine the special properties of nanofibers, many studies[10–13] have focused on electrospinning, which uses an electrical charge to draw fine fibers from a polymer solution. These studies revealed that electrospun mats composed of nanofibers show excellent filtration and absorbability performance. However, nanofiber nonwovens produced by electrospinning are limited in their applications because of their very weak strength and low productivity.

On the basis of previous research[14,15] on the relationship between the transport properties and structural characteristics of conventional needle-punched nonwovens, in this work, we focused on the liquid-transport behavior of needle-punched nonwovens composed of nanofibers produced by conjugate spinning. Three needle-punched nonwovens produced with different stroke numbers and composed

*Correspondence to:* C. W. Joo (changjoo@cnu.ac.kr).
Contract grant sponsor: Welcron R&D Center.
Contract grant sponsor: Ministry of Knowledge Economy in Korea; contract grant number: 10035298.

of poly(ethylene terephthalate) (PET)/co-(polyethylene terephthalate) (Co-PET) sea-island bicomponent fibers were used to prepare the nanofiber nonwovens by an alkali treatment. The objective of this study was to investigate the effect of the pore structure on the water behavior of the needle-punched nanofiber nonwovens and to determine which nanofiber nonwovens had better water absorption capacities and wicking behaviors. Moreover, a theoretical model of air volume and channel radius was established and compared with the experimental results.

### Theoretical approach for calculating the air volume

Liquid absorption capacity is measured from the liquid quantity absorbed by nonwovens in a given time. In a three-dimensional nonwoven structure, the nonwoven volume ($V_n$) is composed of the fiber volume ($V_f$) and the air volume ($V_a$), as shown in Eq. (1). Therefore, the air volume is expressed by Eq. (2):

$$V_n = V_a + V_f \tag{1}$$

$$V_a = V_n - V_f = abT - m/\rho_f \tag{2}$$

where $a$, $b$ and $T$ are length, width and thickness of the nonwovens, respectively. Also, m is nonwoven weight and $\rho_f$ is fiber density.

In this study, the values of air volume of the needle-punched nonwovens composed of bicomponent fibers and nanofibers were calculated by Eq. (2). The calculated values of air volume and the measured values of water absorption capacity of each sample were compared.

### Theoretical approach for calculating the channel radius

For wicking behavior, liquid rises and occupies air volume in nonwoven, similar to liquid absorption. The following assumptions were made to simplify the model for the void structure of the nonwovens:

1. The channels were regarded as a long path from one side of the nonwoven to the other. The length and radius of the channels were the same.
2. The pore shape in the nonwovens was considered to be circle.

A schematic of an ideal needle-punched nonwoven structure, drawn on the basis of these assumptions, is shown in Figure 1. In the structure, the air volume could be considered to be the volume of narrow channels, as shown in Eq. (3):

$$V_a = N_c V_c \tag{3}$$

where $N_c$ is the number of channels. Each channel was composed of pores and was considered to be cylindrical [Eq. (4)]. The tortuosity factor is an important parameter, which determines liquid flow in nonwovens. It is defined as the ratio of the effective channel length to the actual length. Mohannadi et al.[15] provided an equation for the tortuosity factor, where the channel length ($L$) can be calculated:

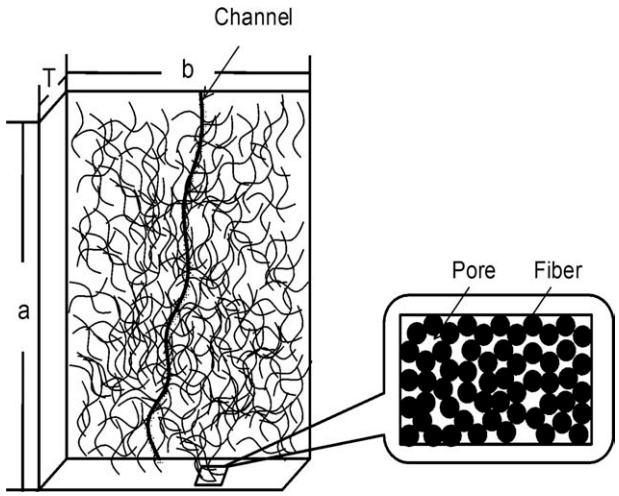


**Figure 1** Schematic of the needle-punched nonwoven structure.

$$V_a = \pi r^2 L \tag{4}$$

Quantifying $N_c$ is important because it reveals the radius of the channel of wicking behavior. Fibers in a nonwoven are randomly and evenly distributed. Thus, the fiber numbers of each cross-sectional area were assumed to be the same and were calculated.[16] The total number of pores could be calculated with Eq. (5):

$$N_p = \frac{4bT - \frac{4m}{\rho_f a}}{\pi D_p^2} \tag{5}$$

where $D_p$ is fiber diameter and $N_p$ is the average number of pores in the cross section of the nonwoven. The total number of channels within the nonwoven was also considered to be $N_p$. In addition, the average channel radius ($r$) was obtained:

$$r = \sqrt{\frac{D_p^2 K a}{4L}} \tag{6}$$

where K is fiber length (51mm).

The radius of the channel is a significant parameter, given that it reveals the ability and height of the wicking behavior. It is calculated by the aforementioned equations. A comparison of the calculated and experimental results for the wicking behavior was analyzed.

**TABLE I**
**Description of Samples**

| Sample ID | Polymer and polymer ratio (wt %) | | Stroke number (number/min) | | Alkali treatment | Basis weight ($g/m^2$) | Thickness (mm) |
|---|---|---|---|---|---|---|---|
| | Sea | Island | Pre | Main | | | |
| A | Co-PET (40) | PET (60) | 400 | 700 | Untreated | 326 | 3.37 |
| B | Co-PET (40) | PET (60) | 800 | 1700 | Untreated | 293 | 2.95 |
| C | Co-PET (40) | PET (60) | 950 | 2500 | Untreated | 276 | 2.33 |
| A1 | — | PET (100) | 400 | 700 | Treated[a] | 192 | 0.73 |
| B1 | — | PET (100) | 800 | 1700 | Treated[a] | 167 | 0.64 |
| C1 | — | PET (100) | 950 | 2500 | Treated[a] | 153 | 0.59 |

[a] Treatment conditions: NaOH concentration = 1%, treatment temperature = 95°C, treatment time = 50 min.

## EXPERIMENTAL

### Material and sample preparation

Three needle-punched nonwovens were fabricated by PET/co-PET bicomponent fibers with different stroke numbers. Nanofiber nonwovens were prepared with the three nonwovens via alkali treatment. The description of the nonwovens and the optimum alkali treatment conditions are summarized in Table I. The nonwoven samples in this study were fabricated by prepunching and main-punching (SH-DDR2500, Samhwa, Gyungsan, Korea) machine. The following parameters were the same in each nonwoven: supply and windup production velocity = 1.6 m/min for prepunching and 2.6 m/min for main punching, distance of plate and bed plate = 15 mm for prepunching and 25 mm for main punching, and needle depth = 8 mm for prepunching and 48 mm for main punching.

### Morphological structures

The morphology of the nonwovens before and after alkali treatment was observed by scanning electron microscopy (SEM; JSM-6300, Tokyo, Japan) at 1 kV. The fiber diameter and its distribution were measured with image analysis software.

### Pore diameter distribution

According to the principle of the liquid extrusion porosimetry technique, the pore diameter distribution of the nonwovens was determined with a capillary flow porosimeter (CFP1200-AEL, PMI, New York, USA). A fully wetted specimen 20 × 20 $cm^2$ in area was placed in the chamber, after which the chamber was sealed. Airflow was allowed into the chamber after the specimen was placed. When the pressure reached a point that could overcome the capillary action of the fluid within the largest pore, a bubble point was found. After the determination of the bubble point, the pressure was increased, and the flow was measured until all of the pores were empty. The airflow pressure and flow rates through the dry specimen were also measured.

### Water absorption capacity

The water absorption capacity depended on the material structure and absorption time. According to the ISO9073-6 standards, the samples were cut into dimensions of 100 × 100 $mm^2$. Each sample had five specimens, and each specimen was larger than 1 g. The test method is explained in detail as follows. First, the specimens were soaked in water for 60 s at room temperature after weighing ($m_1$). The specimens were immersed completely in water, with no part left exposed to air. Then, the specimens were taken out and allowed to stand at room temperature for 120 s until all the water was drained. Finally, they were weighed again ($m_2$). The water absorption capacity is expressed in Eq. (7):

$$\text{Water absorption capacity}(\%) = \frac{m_2 - m_1}{m_1} \times 100 \quad (7)$$

To determine the saturation of the samples, a longer absorption time was also tested.

### Wicking behavior

*Wicking behavior* is described as the ability of water to rise in a thin channel in a nonwoven. It depends on the wicking time and pore structure. According to ISO9073-6, the samples were cut into dimensions of 250 × 30 $mm^2$. Each sample had five specimens each in the machine direction (MD) and cross direction (CD), respectively. Each specimen was tested with the device shown in Figure 2. After 10, 30, 60, 120, 180, 240, and 360 s, the wicking height from the ruler was recorded.

## RESULTS AND DISCUSSION

### Morphological structure

The morphological structure of the nonwovens was characterized by SEM, as shown in Figure 3. Samples

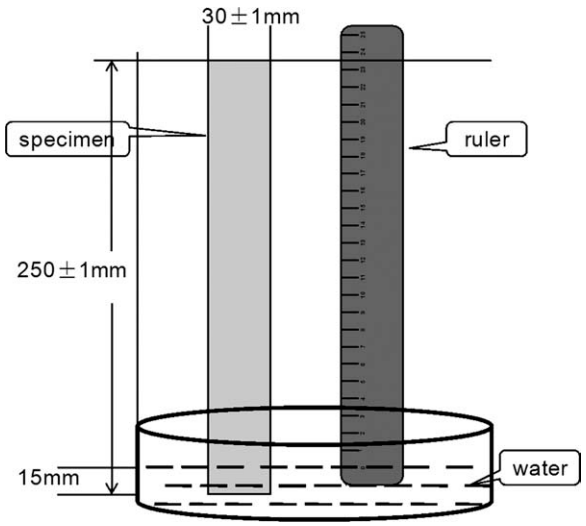


**Figure 2** Device used for the wicking height test.

A, B, and C were nonwovens composed of PET/co-PET sea-island bicomponent fibers. The staple fibers were randomly distributed, and the diameter of the fibers was fixed at 21–23 μm. Samples A1, B1, and C1 were obtained by the treatment of samples A, B, and C in NaOH solution. After complete alkali treatment, co-PET was dissolved in the solution, and the PET nanofibers were separated. One bicomponent fiber was separated into hundreds of fine fibers. Therefore, the fiber diameter significantly decreased to 800–900 nm.

In addition, the micrographs clearly showed that large pores formed in the nonwovens before the alkali treatment. However, after treatment, thousands of nanofibers separated, and the pore size was reduced. Moreover, the specific surface area significantly increased. Thus, nonwovens composed of nanofibers were produced.

### Fiber diameter distribution

The fiber diameters of the nonwoven samples were measured on the basis of the SEM images. Samples A, B, and C were nonwovens composed of PET/co-PET bicomponent fibers. The fiber diameter distributions were similar because they had the same bicomponent fibers. Figure 4 shows the fiber diameter distributions of samples A and A1. The fibers of samples A, B, and C consisted of sea-island bicomponent structures, and their average diameter was 22 μm. During the alkali treatment, however, the sea component was dissolved, and the nanofibers were separated. The fiber diameters of samples A1, B1, and C1 significantly decreased, achieving an average of 880 nm.

### Pore diameter and its distribution

The pore diameter and its distribution were experimentally determined with a capillary flow porosimeter. The values of the mean, maximum, minimum, and most probable pore diameter were obtained on the basis of the experiment. A comparison was made between the calculated and experimental results for the various pore diameters of the nonwovens (Table II). The calculated value of the mean pore diameter was determined with the Bryner model.[17] Significant decreases were observed in the calculated mean pore diameter and experimental

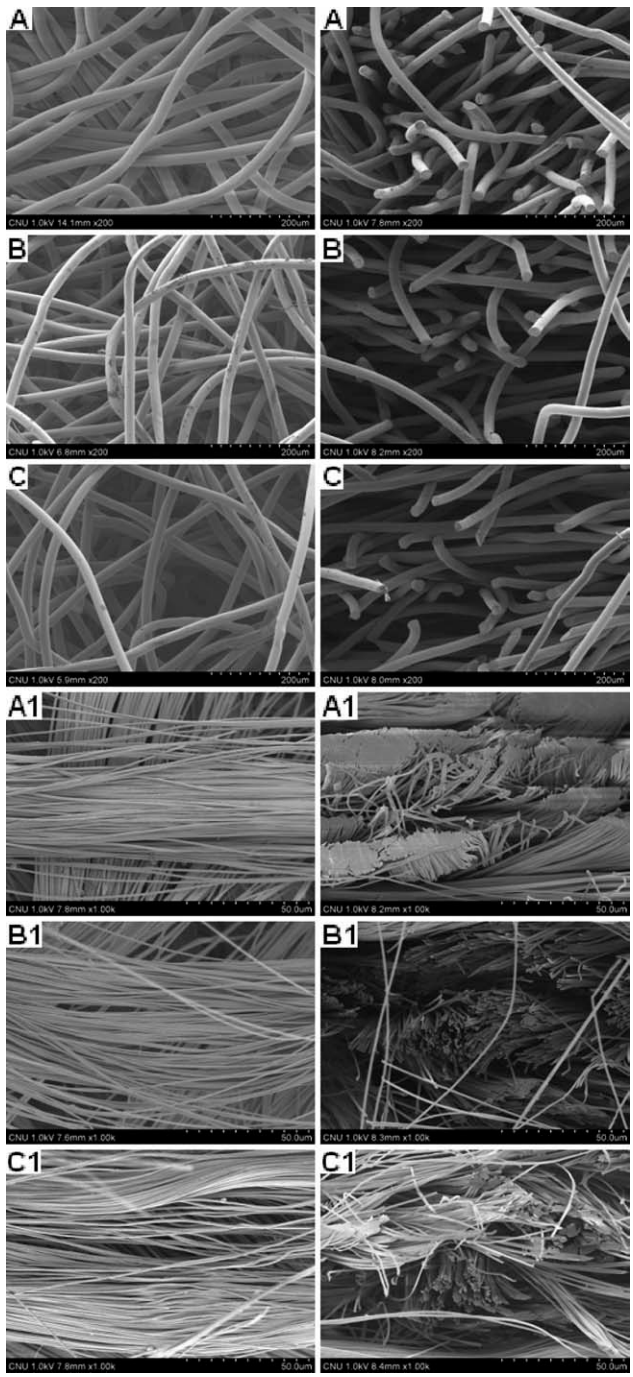


**Figure 3** SEM images of the surfaces and cross sections of nonwovens (200× magnification for bicomponent fibers and 1000× magnification for nanofibers).

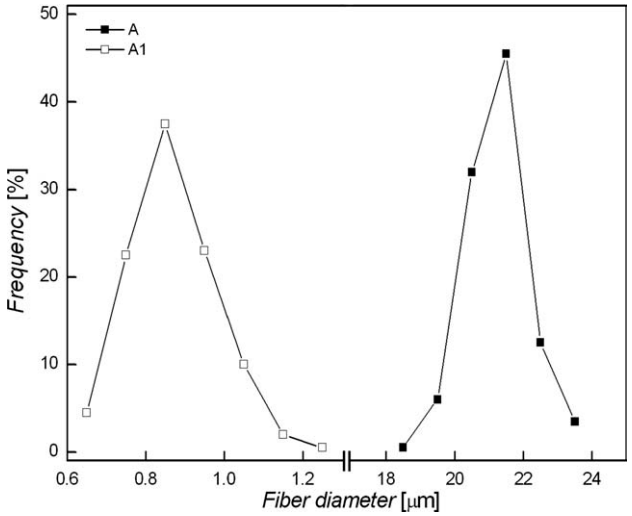


**Figure 4** Fiber diameter distributions of the untreated and treated nonwovens (samples A and A1).

mean, maximum, minimum, and most probable pore diameters of the nonwovens treated in NaOH solution. The pore diameter was proportional to the fiber diameter of the nonwovens. After alkali treatment, the bicomponent fibers were separated into nanofibers, and the fiber diameter decreased to 96%. The nanofibers were redistributed during treatment; this caused nonwoven shrinkage. Thus, the pore diameter decreased significantly to 88%. In addition, nonwoven samples A, B, and C were fabricated with different stroke numbers. As the stroke number increased, the punch density of the nonwovens also increased. This result indicated that theoretically, the pore size of sample C was the smallest among the three samples. According to the calculated results, the pore diameter decreased slightly with increasing stroke number. However, the trend was not visibly observed in the experimental results. This occurrence may have been due to overlapping among the pores and the irregularity of the pore area.

The comparison between the pore diameter distributions of the nonwovens composed of bicomponent and nanofibers is shown in Figure 5. The pore diameter distributions of samples A, B, and C visibly followed a wider distribution compared with those of samples A1, B1, and C1, which followed a narrow distribution. The pore diameter distribution of the untreated samples was 60% from 40 to 80 μm. Meanwhile, the pore diameter distributions of the treated samples were distributed at more than 80% from 5 to 10 μm. The nonwovens composed of nanofibers showed a compact and uniform textile structure. The pore diameter distribution is one of the most important factors in the evaluation of the liquid absorption properties of nonwovens. A smaller pore diameter causes faster liquid absorption.

Therefore, the pore structure, including the total volume of the pores, the pore diameter, and the distribution, is the most important structural parameter that controls the transport behavior in nonwovens. The aforementioned discussion indicates that the nonwovens composed of nanofibers have promising potential applications as absorption media.

### Water absorption capacity

The absorbency process during the water absorption test is described as follows. First, water gradually entered from the nonwoven surface into the nonwoven interior through the pores in the nonwovens. Then, the water permeated into the nonwoven interior and came into contact with the fibers of the nonwoven interior. When the air volume of the nonwoven was filled with water, the fibers stopped to absorb the water, and the nonwoven reached saturation. The experimental results for the water absorption behavior of the nonwovens composed of bicomponent fibers as a function of the absorption time are shown in Figure 6. With increasing absorption time, the weight of absorbed water also increased, and the samples reached saturation in 5 min. However, the nonwovens composed of nanofibers reached saturation only in 1 min.

The water absorption capacities of the nonwovens composed of bicomponent fibers and nanofibers were calculated with Eq. (7). These were compared, and the results are shown in Figure 7. The water absorption capacities of the samples were calculated under saturation conditions. A better water absorption ability and a higher water absorption speed in

**TABLE II**
**Comparison of Experimental and Calculated Results for the Pore Diameter**

| Sample ID | Experimental (μm) | | | | Calculated (μm) |
|---|---|---|---|---|---|
| | Mean | Maximum | Minimum | Most probable | Mean |
| A | 66.91 | 121.73 | 33.52 | 35.78 | 118.70 |
| B | 65.24 | 113.08 | 38.03 | 38.03 | 117.81 |
| C | 69.99 | 126.48 | 37.01 | 50.71 | 115.64 |
| A1 | 8.00 | 19.68 | 1.91 | 3.39 | 1.91 |
| B1 | 8.93 | 25.56 | 3.78 | 5.24 | 1.96 |
| C1 | 7.72 | 23.59 | 2.78 | 3.82 | 1.78 |

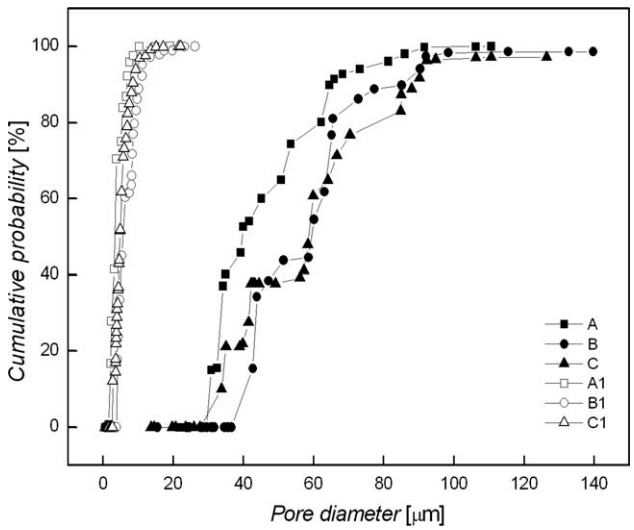


**Figure 5** Pore diameter distributions of the untreated and treated nonwovens.

the nanofiber nonwovens were observed because the nanofiber nonwovens reached saturation in only 1 min, whereas the nonwovens composed of bicomponent fibers reached saturation in at least 5 min. This was further observed through a comparison of their water absorption capacities per volume. After alkali treatment, the water absorption capacities per volume of samples A1, B1, and C1 increased by 181.5, 218.2, and 161.0%, respectively. The water absorption behavior was driven by the capillary pressure in the nonwovens. The pore diameters of the nanofiber nonwovens were smaller than those of the nonwovens composed of bicomponent fibers. The smaller pore diameter caused a higher capillary pressure; this resulted in rapid water absorption.

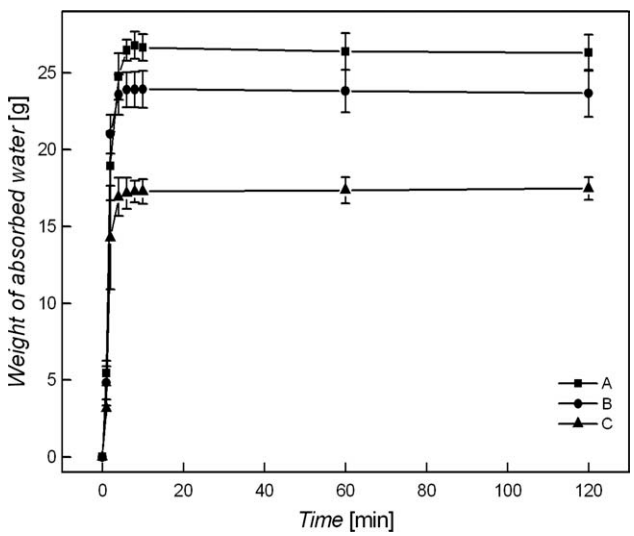


**Figure 6** Water absorption behavior of the untreated nonwovens with absorption time.

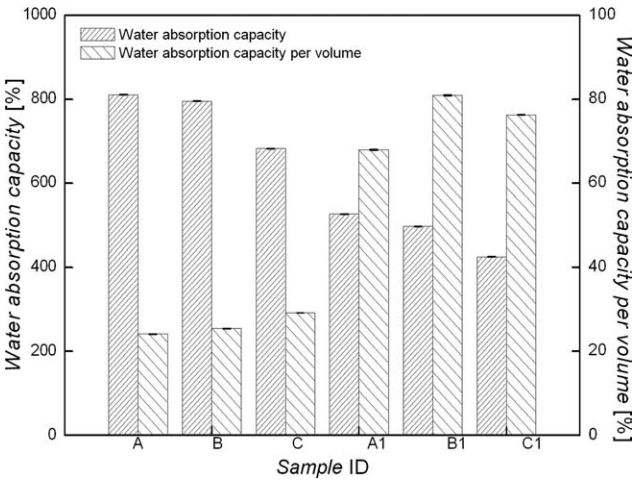


**Figure 7** Comparison of the water absorption capacities of the untreated and treated nonwovens.

The *water absorption behavior* refers to the water occupying the air volume of a nonwoven as it absorbs water. In this study, the air volume in the sample was calculated with Eq. (2). A comparison of the calculated results for air volume and the experimental results for absorbed water volume is shown in Figure 8. For samples A, B, and C, the experimental results for water volume during saturation were obtained from Figure 6. The calculated results for air volume were larger than the experimental results for absorbed water volume because of the pore structure. In the nonwovens composed of bicomponent fibers, the pore diameter was so large that the pores could not hold water in the nonwovens. During sample removal from the water, the absorbed water dripped continuously, and as a result, the value of the absorbed water volume was dramatically lower than that of the air volume.

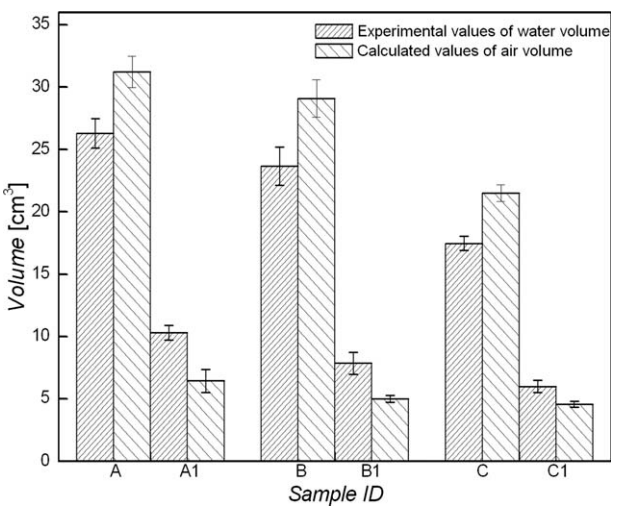


**Figure 8** Comparison of the air volume and absorbed water volume of the untreated and treated nonwovens.

However, the nonwovens composed of nanofibers possessed fast water absorption properties. On the basis of the previous results, they reached saturation in 1 min. As Figure 8 shows, the calculated results for air volume were lower than the experimental results for water volume because of the pore structure as well. The nonwovens composed of nanofibers expanded in terms of length and width when the samples absorbed water.[18] The smaller pore diameter was conducive to water absorption because of capillary action. It caused the absorbed water volume to increase beyond the calculated air volume.

The difference among samples A, B, and C was the increasing punch density, which was due to rising stock number. This result indicates decreases in the value of both the absorbed water volume and the calculated air volume of samples A, B, and C (Fig. 8). The same trend was observed for the punch density of samples A1, B1, and C1.

### Wicking behavior

*Wicking behavior* is the ability of a liquid to flow against gravity, in which the liquid spontaneously rises in a narrow channel composed of a porous structure in nonwovens. The wicking heights of the nonwovens composed of the bicomponent fibers and nanofibers were measured. Figure 9 shows the results for samples B and B1 in the MD and CD. In each sample, the wicking height gradually increased as the experimental time lengthened. The wicking height of the alkali-treated nonwoven samples was significantly higher than that of the untreated samples. The results were in agreement with the water absorption property results because of the smaller pore diameter of the nonwovens composed of nanofibers.

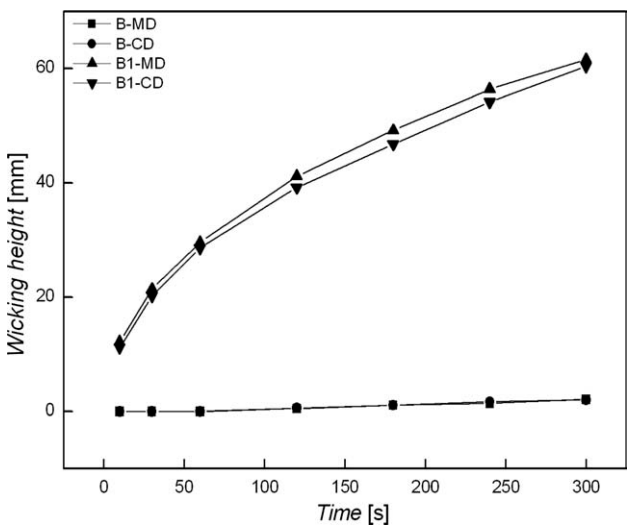


**Figure 9** Wicking behaviors of the nonwovens in MD and CD (samples B and B1).

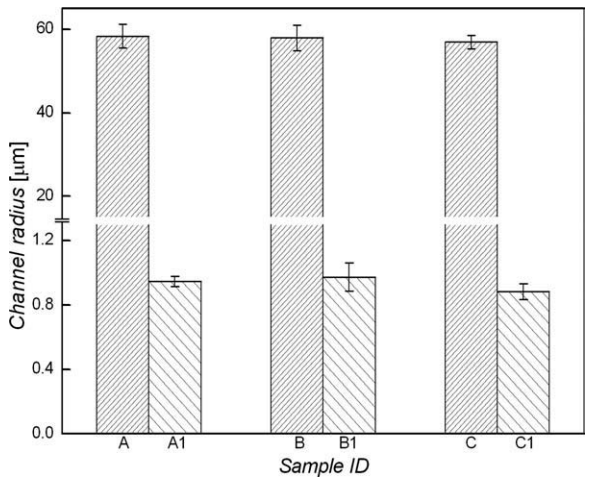


**Figure 10** Calculated values of the channel radius of the untreated and treated nonwovens.

According to Poiseuille's law,[19] the capillary force was high because of the small pore diameter, which caused a higher wicking height. Moreover, these figures clearly showed no significant influence of direction on the wicking behavior of the nonwoven samples. The wicking behavior was related to the pore structure, that is, the pore diameter and porosity, which were not dependent on the direction; this showed that the nonwoven structure was a random and uniform textile structure.

Meanwhile, the channel radius was calculated with Eq. (6) on the basis of the nonwoven structure. The results are shown in Figure 10. Compared with the pore diameters in Table II, good correlation was achieved among the experimental values of the maximum pore diameter, calculated values of the pore diameter, and channel radius in the untreated nonwovens. The channel radii were in the range 55–60 μm. For the alkali-treated samples, however, similar values were observed among the experimental values of mean, minimum, and most probable pore diameter, as well as the calculated values of the mean pore diameter and channel radius in the nonwovens. The channel radius significantly decreased to less than 1 μm because of the nanofibers in the treated nonwovens. After alkali treatment, the fiber diameter decreased by 95.9%. It was directly affected by the reduction (98.36%) in the channel radius. Thus, the nonwovens composed of nanofibers possessed excellent wicking behavior because the capillary action was high, given the very small channel radius.

## CONCLUSIONS

Needle-punched nonwovens composed of nanofibers were prepared by nonwovens based on PET/co-PET bicomponent fibers by alkali treatment. After treatment, co-PET was dissolved in the alkali solution,

and the PET nanofibers were separated. The fiber diameter significantly decreased from 22 μm to 880 nm. The pore diameter distributions of the untreated nonwovens followed a wider distribution compared with those of the nonwovens composed of nanofibers, which followed a narrow distribution. The experimental and calculated mean pore diameters visibly decreased by 87.8 and 98.4%, respectively, because of the fiber diameter reduction of 96.0%.

The water absorption behavior of the needle-punched nonwovens based on different pore structures was also investigated. With increasing absorption time, the untreated nonwovens reached saturation after 5 min. However, the nonwovens composed of nanofibers reached saturation in only 1 min. This result indicates the excellent water absorption capacity of the nonwovens composed of nanofibers. The comparison of samples A, B, and C and A1, B1, and C1 showed decreases both the absorbed water volume and calculated air volume. This phenomenon was attributed to the gradual increase in the punch density; this indicated that samples C and C1 had a compact nonwoven structure.

Moreover, the nonwovens with a smaller pore diameters possessed faster wicking speeds than the untreated nonwovens in both the MD and CD. The channel radius was calculated, and the values of the untreated and treated nonwovens were 55–60 μm and less than 1 μm, respectively. After alkali treatment, the fiber diameter decreased by 95.9%. It was directly affected by the reduction in the channel radius of 98.36%. Thus, the nonwovens composed of nanofibers possessed excellent water absorption behavior and wicking behavior because the capillary action was high given the smaller pore size.

## References


1. Russell, S. J. Handbook of Nonwovens; Woodhead: Cambridge, England, 2007; Chapter 5, p 223–240.
2. Rawal, A. J Text Inst 2010, 101, 350.
3. Kotharia, V. K.; Agarwala, G. J Ind Text 2007, 98, 317.
4. Zhu, Q.; Li, Y. Int J Heat Mass Transfer 2003, 46, 5099.
5. Anantharamaiah, N.; Verenich, S.; Pourdeyhimi, B. J Eng Fiber Fabrics 2008, 3, 1.
6. Sun, C.; Zhang, D.; Liu, Y. B.; Xiao, R. J Appl Polym Sci 2004, 93, 2090.
7. Ndaro, M. S.; Jin, X. Y.; Chen, T.; Yu, C. W. Fiber Polym 2007, 8, 421.
8. Duan, J. L.; Teng, C. Q.; Han, K. Q.; Yu, M. H.; Wu, W. X.; Zhang, Q. J.; Chiang, K. S. Polym Eng Sci 2009, 49, 1671.
9. Gong, R. H.; Nikoukhesal, A. Polym Eng Sci 2009, 49, 1703.
10. Ryu, Y. J.; Kim, H. Y.; Lee, K. H.; Park, H. C.; Lee, D. R. Eur Polym J 2003, 39, 1883.
11. Gibson, P.; Schreuder-Gibson, H.; Rivin, D. Colloids Surf A 2001, 187–188, 469.
12. Barhate, R. S.; Loong, C. K.; Ramakrishna, S. J Membr Sci 2006, 283, 209.
13. Holzmeister, A.; Rudisile, M.; Greiner, A.; Wendorff, J. H. Eur Polym J 2007, 43, 4859.
14. Rawal, A. J Text Inst 2006, 97, 527.
15. Mohammadi, M.; Lee, P.; Ghadimi, P. J Ind Text 2002, 32, 45.
16. Li, Y.; Joo, C. W. Fiber Polym, to be publish as accepted paper.
17. Simmonds, G. E.; Bomberger, J. D.; Bryner, M. A. J. Eng Fiber Fabrics 2007, 2, 1.
18. Hansen, L. M.; Smith, D. J.; Reneker, D. H.; Kataphinan, W. J Polym Sci 2005, 95, 427.
19. Schoenmaker, B. D.; Schueren, L. V.; Vrieze, S. D.; Philippe, W.; Karen, D. C. J Appl Polym Sci 2011, 120, 305.